RESEARCH ARTICLE | *Obesity, Diabetes and Energy Homeostasis*

Obesity-induced vascular inflammation involves elevated arginase activity

Lin Yao,[1,2]* Anil Bhatta,[2]* Zhimin Xu,[3] Jijun Chen,[2] Haroldo A. Toque,[2] Yongjun Chen,[7] Yimin Xu,[3] Zsolt Bagi,[3,4] Rudolf Lucas,[2,3,4] Yuqing Huo,[3,5] Ruth B. Caldwell,[3,5,6] and R. William Caldwell[2,3]

[1]*School of Pharmaceutical Sciences, South China Research Center for Acupuncture and Moxibustion, Guangzhou University of Chinese Medicine, Guangzhou, People's Republic of China;* [2]*Department of Pharmacology and Toxicology, Medical College of Georgia, Augusta University, Augusta, Georgia;* [3]*Vascular Biology Center, Medical College of Georgia, Augusta University, Augusta, Georgia;* [4]*Department of Medicine, Medical College of Georgia, Augusta University, Augusta, Georgia;* [5]*Department of Cell Biology and Anatomy, Medical College of Georgia, Augusta University, Augusta, Georgia;* [6]*Veterans Administration Medical Center, Augusta, Georgia; and* [7]*South China Research Center for Acupuncture and Moxibustion, Guangzhou University of Chinese Medicine, Guangzhou, People's Republic of China*

Yao L, Bhatta A, Xu Z, Chen J, Toque HA, Chen Y, Xu Y, Bagi Z, Lucas R, Huo Y, Caldwell RB, Caldwell RW. Obesity-induced vascular inflammation involves elevated arginase activity. *Am J Physiol Regul Integr Comp Physiol* 313: R560–R571, 2017. First published August 23, 2017; doi:10.1152/ajpregu.00529.2016.—Obesity-induced vascular dysfunction involves pathological remodeling of the visceral adipose tissue (VAT) and increased inflammation. Our previous studies showed that arginase 1 (A1) in endothelial cells (ECs) is critically involved in obesity-induced vascular dysfunction. We tested the hypothesis that EC-A1 activity also drives obesity-related VAT remodeling and inflammation. Our studies utilized wild-type and EC-A1 knockout (KO) mice made obese by high-fat/high-sucrose (HFHS) diet. HFHS diet induced increases in body weight, fasting blood glucose, and VAT expansion. This was accompanied by increased arginase activity and A1 expression in vascular ECs and increased expression of tumor necrosis factor-α (TNF-α), monocyte chemoattractant protein-1 (MCP-1), interleukin-10 (IL-10), vascular cell adhesion molecule-1 (VCAM-1), and intercellular adhesion molecule-1 (ICAM-1) mRNA and protein in both VAT and ECs. HFHS also markedly increased circulating inflammatory monocytes and VAT infiltration by inflammatory macrophages, while reducing reparative macrophages. Additionally, adipocyte size and fibrosis increased and capillary density decreased in VAT. These effects of HFHS, except for weight gain and hyperglycemia, were prevented or reduced in mice lacking EC-A1 or treated with the arginase inhibitor 2-(S)-amino-6-boronohexanoic acid (ABH). In mouse aortic ECs, exposure to high glucose (25 mM) and Na palmitate (200 μM) reduced nitric oxide production and increased A1, TNF-α, VCAM-1, ICAM-1, and MCP-1 mRNA, and monocyte adhesion. Knockout of EC-A1 or ABH prevented these effects. HFHS diet-induced VAT inflammation is mediated by EC-A1 expression/activity. Limiting arginase activity is a possible therapeutic means of controlling obesity-induced vascular and VAT inflammation.

arginase; endothelial cell activation; inflammation; macrophage; obesity

OBESITY IS A MAJOR risk factor for the development of type 2 diabetes (21) and cardiovascular disease. Diabetes and obesity-induced vascular dysfunctions are characterized by an array of blood flow reducing pathologies, including impaired vasorelaxation, increased stiffening, and microvascular rarefaction (2, 6, 15, 22, 24, 37, 42, 46). In obesity and type 2 diabetes, excessive accumulation of adipose tissue is strongly associated with macrophage infiltration and chronic low-grade inflammation (45, 48). Obesity-induced inflammation is thought to result from pathological expansion and fibrosis of visceral adipose tissue (VAT) (29) in a context of vascular rarefaction and reduced blood flow, leading to hypoxia, adipocyte death, and activation of resident immune cells, which release inflammatory mediators. Inflammatory macrophages are a major source of reactive oxygen species (ROS) and proinflammatory cytokines. Hypoxia, ROS, and inflammatory cytokines all contribute to elevated expression and activity of the urea hydrolase enzyme arginase (6, 20, 44, 52). Previous studies in models of obesity have shown that activity of arginase plays a critical role in the inflammatory process (17, 19).

Arginase, which catalyzes the hydrolysis of L-arginine to urea and L-ornithine, has been implicated in many cardiovascular diseases, including diabetes (37). Arginase can reciprocally regulate production of nitric oxide (NO) by NO synthase (NOS) through competition for their common substrate, L-arginine (33, 37). Elevated arginase activity can reduce NO production by NOS, and uncouple NOS, causing it to produce more ROS (superoxide and peroxynitrite) (28). This process can further activate arginase and other ROS generators resulting in a feed forward exacerbation of the oxidative stress (6, 32). There are two arginase isoforms: arginase 1 (A1), cytoplasmic and highly expressed in the liver, and arginase 2 (A2), largely mitochondrial, and the primary renal isoform. Both are found in vascular tissue. A1 also is found in anti-inflammatory M2-like macrophages involved with reparative functions (27), and A2 is reported to be present in proinflammatory and cytotoxic M1-like macrophages (50). Obesity and type 2 diabetes can induce vascular inflammation and dysfunction in several animal models, such as Zucker obese and diabetic rats (19, 31) and *db/db* mice (35). Arginase was shown to be involved in the vascular dysfunction of Zucker obese rats (19). A previous study of mice fed a high-fat/high-sucrose (HFHS) diet for 6 mo demonstrated vascular endothelial dysfunction, reduced NO levels, and enhanced vascular fibrosis and stiffness, as well as increased vascular and systemic oxidant stress

---

* L. Yao and A. Bhatta contributed equally to this work.

Address for reprint requests and other correspondence: R. W. Caldwell, Dept. of Pharmacology and Toxicology, Medical College of Georgia, Augusta Univ., Augusta, GA 30904 (e-mail: wcaldwel@augusta.edu).

and elevated arginase expression/activity in a condition of obesity and hyperglycemia. Specific absence of A1 in endothelial cells (ECs) or treatment with an arginase inhibitor prevented all of these developments except obesity and hyperglycemia (4). Our present study was performed to assess the involvement of endothelial expression of A1 in obesity-induced inflammation and pathological remodeling of the VAT. We hypothesized that VAT dysfunction is selectively driven by A1-mediated EC dysfunction, which subsequently leads to VAT inflammation, fibrosis, and related vascular pathologies.

MATERIALS AND METHODS

Animals. Animal protocols were approved by the Institutional Animal Care and Use Committee at Augusta University. Male C57BL/6J mice (Jackson Laboratory, Bar Harbor, ME) were used. The mice were either wild-type (WT) or those with an EC-specific knockout of A1 (EC-A1$^{-/-}$). Mice that expressed Cre-recombinase in ECs (Cadherin 5-Cre, Stock No. 017968) were crossed with mice that carried floxed A1 alleles (loxP sites flanking exons 7 and 8 of the A1 gene, Stock No. 008817) to generate EC-specific A1 knockout mice (EC-A1$^{-/-}$). A1$^{loxp/loxp}$ (EC-A1$^{+/+}$) mice, which have the same phenotype as C57BL/6J WT mice, were used as controls for the knockout and are referred to as A1^{con}. Mice were maintained for 6 mo on a high-fat/high-sucrose (HFHS) diet [percentage of calories: 59% fat, 15% protein, and 26% carbohydrate (20% from sucrose); No. F1850; BioServe] or a normal diet [ND; percentage of calories: 18% fat, 24% protein, and 58% carbohydrate (~45% from sucrose); Harlan]. Groups of WT mice on ND or HFHS diet also were treated with the arginase inhibitor 2-(S)-amino-6-boronohexanoic acid (ABH) at a dose of 10 mg·kg^{-1}·day^{-1} in the drinking water starting 1 mo after the beginning the diets and continuing for 5 mo. Body weight and blood/urine glucose levels of each mouse were measured every 2 wk until experiments were performed. Animals were housed in 12-h light-dark cycle and had free access to food and water throughout the study. After 6 mo on the HFHS or ND, animals were anesthetized with ketamine HCl (100 mg/kg) and xylazine (10 mg/kg ip). When adequacy of anesthesia was reached as indicated by the disappearance of pedal withdrawal reflex, blood was collected, and aorta tissue and epididymal VAT were harvested and placed in PBS.

Measurement of ABH in plasma samples. For calibration, ABH was mixed with blank plasma and incubated with gentle shaking at 37°C for 1 h. Acetonitrile was added to plasma in a 3:1 volume ratio, and the mixture was vortexed for 1 min and then centrifuged at 14,000 rpm for 20 min at 4°C to extract the ABH and remove proteins. The acetonitrile was passed through a 0.22-μm filter and assayed. Samples from WT mice given ABH for 5 mo were processed in the same manner.

ABH in plasma was detected by HPLC (SHIMADZU LC-30AD) with an evaporative light-scattering detector (Alltech 6000). The mobile phase comprised 0.1% trifluoroacetate acid (*solution A*) and acetonitrile (*solution B*) by using gradient elution of *solution B* from 5 to 60% (vol/vol) over 20 min, and the flow rate was 1 ml/min. The stationary phase was a C18 reverse-phase column (250 × 4.6 mm, 5 μm; LabChrom). The nitrogen flow rate was 0.5 l/min, The retention time of the ABH standard was 4.25 min.

WT mice given ABH at a dose rate of 10 mg·kg^{-1}·day^{-1} in the drinking water for 5 mo exhibited an average ABH plasma concentration of 0.27 ± 0.02 mmol/l ($n = 6$). ABH inhibits both isoforms arginase (1, 2) with similar potencies and would inhibit both at this concentration (5).

Isolation of ECs from aorta of HFHS and ND-fed mice. Whole aorta tissue was excised and perfused with 1 ml of PBS containing 1,000 U/ml of heparin to remove the blood. The fat or connecting tissue was rapidly removed and a 24-gauge cannula was inserted into the proximal portion of the aorta. After ligation of that site with silk

thread, the lumen was briefly washed with serum-free DMEM. The other end was filled with collagenase type II solution (2 mg/ml, in serum-free DMEM) and closed with silk thread. After incubation for 45 min at 37°C, ECs were removed by flushing the aortic lumen with 5 ml of DMEM containing 20% FBS and then centrifuged at 1,200 rpm for 5 min. Flushed cells were purified by Dynabeads FlowComp Flexi (Invitrogen) with CD31 antibody (Thermo Scientific).

ELISA method for measurement of protein levels. Total proteins were extracted by RIPA buffer from isolated aortic ECs. After centrifugation, protein pellets were collected. After dilutions, the final protein concentration of samples was 3 mg/ml. Samples were assayed with the following ELISA kits: TNF-α (EMC102a; Neobioscience, Guangdong, China), monocyte chemoattractant protein-1 (MCP-1; EMC113; Neobioscience), IL-10 (EMC005; Neobioscience), ICAM1 (CD54; ab100688; Abcam), and VCAM1 (ab100750; Abcam).

Isolation of stromal vascular fraction. Epididymal adipose tissue was excised, rinsed in saline, minced, and digested with collagenase (Roche) at 37°C for 1 h. Tissue was washed with HEPES-DMEM buffer (15 mM HEPES, 10 mg/ml fatty acid-poor BSA, and 0.5 mM CaCl$_2$) and centrifuged at 1,500 rpm for 5 min. Collected tissues were incubated in 1 ml collagenase HEPES-DMEM (collagenase concentration of 1 mg/ml) at 37°C for 1 h. The suspension was filtered through 10-μm filters and centrifuged at 1,500 rpm for 5 min at room temperature. The cellular pellets of stromal vascular fraction (SVF) were used for the experiments.

Quantitative reverse transcription-PCR. Total RNA from the aorta and the SFV of the VAT was isolated using TRIzol reagent (Invitrogen). Total RNA was reverse transcribed with Moloney murine leukemia virus reverse transcriptase (Invitrogen) to generate cDNA. Gene expression was determined by quantitative PCR with SYBR Green Dye Gene Expression Assays (for TNF-α, IL-10, VCAM-1, ICAM-1, and MCP-1) or TaqMan Gene Expression Assays (for A1; Applied Biosystems), which was performed on a StepOne Plus thermocycler (Applied Biosystems). Primer sequences are presented in Table 1. The cycle threshold, determined as the initial increase in fluorescence above background, was determined for each sample. Hypoxanthine phosphoribosyl transferase was used as internal control in the PCR reaction for normalization of assays.

Flow cytometry. A Becton Dickinson FACS Calibur flow cytometer was used for flow cytometry analyses of cells from the blood and SVF. Circulating inflammatory monocytes were measured as phycoerythrin (PE)-conjugated anti-F4/80 (Cedarlane)-positive/allophycocyanin (APC)-conjugated anti-Ly6c-positive (BD PharMingen) (12). M1- or M2-like macrophages from the SVF were identified as PE-conjugated anti- F4/80 (PE; Cedarlane)-positive/APC-conjugated anti-CD11c (BD PharMingen)-positive/FITC-conjugated anti-CD206 (BD PharMingen)-negative or F4/80-positive/CD11c-negative/CD206-positive cells, respectively (13). The numbers of M1- or M2-like macrophages were calculated by multiplying the number of trypan blue-negative cells by the ratio of F4/80-positive/CD11c-positive/CD206-negative cells or that of F4/80-positive/CD11c-negative/CD206-positive cells. Appropriate unspecific isotypes were used as controls (BD PharMingen).

Morphometric analysis of VAT. Freshly dissected epididymal VAT was excised from mice and placed in paraformaldehyde (4%) over-

Table 1. *Primer sequences for expression of genes*

No.	Target	Forward (5′-3′)	Reverse (5′-3′)
1	ICAM-1	CAGTCCGCTGTGCTTTGAGA	CGGAAACGAATACACGGTGAT
2	VCAM-1	CTGGGAAGCTGGAACGAAGT	CAGGGGGCCACTGAATTGAA
3	MCP-1	GGCTCAGCCAGATGCAGTTAA	CCTACTCATTGGGATCATCTTGCT
4	Ets-1	TATCATCCACAAGACGGCGG	GGCTTTACATCCAGCATGGC
5	TNF-α	GCTCTTACTGACTGGCATGAG	CGCAGCTCTAGGAGCATGTG
6	IL-10	GCTCTTACTGACTGGCATGAG	CGCAGCTCTAGGAGCATGTG

MCP-1, monocyte chemoattractant protein-1.

night before being washed and placed in 70% EtOH for short storage. The VAT was then embedded in paraffin and cut into 5-μm sections for histochemical analysis. Sections were stained with Masson-trichrome for analysis of collagen levels (fibrosis) and determination of adipocyte size. Sections also were stained for ECs (Isolectin B4; ThermoFisher) marker or macrophage (mouse MAC-2 antibody; Accurate Chemical & Scientific). Crown-like structures (macrophage around degenerating adipocytes) were quantified (5 images/group).

EC culture and treatments. Mouse aortic endothelial cells (MAECs) were purchased from Cell Applications (San Diego, CA), cultured in mouse aortic EC growth medium (Cell Applications), and maintained in a humidified atmosphere at 37°C and 5% CO_2. All experiments were performed with cells from passage 4–8. The L-arginine and serum concentrations were adjusted before treatment using M-199 media (Invitrogen) containing 0.2% FBS, 50 μM L-arginine, 100 U/ml penicillin, 100 μg/ml streptomycin, and L-glutamine. This L-arginine concentration (50 μM) is comparable to normal plasma arginine levels (40–100 μM). MAECs were exposed to media containing either normal glucose concentration (NG; 5.5 mM) and BSA or high-glucose concentration (HG; 25 mM) and BSA-conjugated palmitate (PA; 200 μM) for 48 h. Cells were treated with the arginase inhibitor ABH (100 μM) for 1 h before the HG + PA treatment.

CRISPR/Cas target sites and vector construction. CRISPR target sites were identified using http://crispr.mit.edu/ as described previously (36). The small guide RNA (sgRNA) sequence for A1 was as follows: GTATGACGTGAGAGACCACG. To construct CRISPR/Cas plasmids for AI targeting, sgRNA oligos were synthesized by Invitrogen and cloned into pX330 (Addgene: plasmid no. 42230) vector. This product is pX330-sgARG1. We followed the Zhang laboratory protocol (https://www.addgene.org/crispr/zhang/).

Transfection of MAECs with A1 sgRNA. MAECs were transfected with CRISPR/Cas plasmid pX330-sgARG1 [single-guide (sg)RNA] or control plasmid pX330 using Gene Pulser electroporation buffer reagent (Bio-Rad), according to the manufacturer's instructions. In brief, cells were transfected with 100 nmol/l of plasmids for 5 h by Gene Pulser X cell electroporation system. Transfected cells were collected and cultured for monocyte adhesion studies described below.

NO production. Production of NO was measured using a Sievers 280i NO Analyzer. Fresh control or treated media (1 ml) were applied to MAEC cultures (6-well plates) and collected after 48 h of exposure. Aliquots were injected in glacial acetic acid containing sodium iodide in the reaction chamber. NO_2^- is quantitatively reduced to NO under these conditions, which was quantified by a chemiluminescence detector after reaction with ozone. Addition of the NOS inhibitor nitro-L-arginine methyl ester (L-NAME; 100 μM) to control cultures reduced NO production by ~90%.

Western blot. Lysates from MAEC homogenates (20 μg protein) were subjected to electrophoresis on 10% SDS-polyacrylamide gels. Proteins were electroblotted onto PVDF membranes (Millipore). The blots were blocked with 5% BSA (BSA Fraction V; OmniPur) in TBST (0.2% Tween 20 in 1× Tris-buffered saline). Membranes were incubated with primary antibodies [anti-A1, 1:10,000 (kind gift of Dr. Sidney M. Morris, Jr., University of Pittsburgh), Aves Laboratories, Tigard, OR; and anti-β-actin, 1:4,000, Sigma-Aldrich] prepared in 5% BSA solution overnight at 4°C, washed (3× TBST), and incubated in

secondary antibodies conjugated with horseradish peroxidase for 1 h at room temperature. Signals were detected using chemiluminescence and analyzed using densitometry.

Arginase activity assay. MAECs were frozen in liquid nitrogen and then pulverized in lysis buffer (50 mM Tris·HCl, 0.1 mM EDTA, and EGTA, pH 7.5) containing protease inhibitors. The resultant lysate was subjected to three freeze-thaw cycles and centrifuged at 14,000 rpm for 10 min. The supernatant was collected. Arginase activity was measured by colorimetric determination of urea formed from L-arginine as previously described (9). Briefly, the supernatant fraction (25 μl) was heated with 25 μl $MnCl_2$ (10 mM, 10 min, 56°C) to activate arginase. The mixture was then incubated with 50 μl of 0.5 M L-arginine (pH 9.7) at 37°C for 1 h. The reaction was stopped by adding acid; the solution was then heated at 100°C with 25 μl α-isonitroso-propiophenone (9% α-ISPF in ethanol) for 45 min. Samples were kept in the dark at room temperature for 10 min, and absorbance was then measured at 540 nm. Enzyme activity was normalized to the amount of protein assessed by Bradford protein assay.

Monocyte EC adhesion assay. MAECs (8×10^4–12×10^4/well) were seeded in 12-well flat-bottom plates and maintained for 24 h (until 80% confluent), followed by incubation with HG + PA or NG media for 48 h. After the treatment, media were removed by being washed with PBS and human monocytes (2.5–5×10^5/well-THP-1 cell line; ATCC, Manassas, VA) were added to MAECs after being stained with calcein AM (0.5 ul in 1 ml serum free medium) in the dark, 37°C for 30 min. The cells were allowed to adhere at 37°C for 45 min in PBS. Nonadherent cells were removed by being washed with PBS three times. Monocytes adhering on the endothelial surface (5 fields per culture) were counted under the microscope.

Drugs and chemicals. The arginase inhibitor ABH was a kind gift from Corridor Pharmaceuticals (Baltimore, MD). Sodium palmitate was purchased from Sigma-Aldrich (CAS No. 408-35-5). L-NAME (HCl) was purchased from Cayman Chemical (CAS No. 51298-62-5).

Statistical analysis. Data are presented as means ± SE. Statistical analysis was performed using ANOVA with a Tukey posttest. $P < 0.05$ was taken as significant. These analyses were performed using GraphPad Prism, version 4.00 (GraphPAD Software).

RESULTS

Effects of arginase inhibition or A1 deletion in ECs on diet-induced obesity. After 6 mo of HFHS feeding, WT mice had significant increases in body weight and fasting blood glucose levels as compared with ND-fed mice (52 ± 2 vs. 38 ± 1 g and 11.2 ± 0.9 vs. 6.2 ± 0.2 mmol/l, respectively). The effects of HFHS diet on weight gain and hyperglycemia were not altered by treatment with the arginase inhibitor ABH (10 mg·kg^{-1}·day^{-1} in drinking water) or deletion of A1 in ECs. The HFHS diet also significantly increased the epididymal fat pad weight as a percentage of body weight similarly in WT and A1^{con} mice as compared with ND-fed controls (from ~3.5 to 6%, Table 2). This effect also was not altered by arginase inhibition or lack of EC-A1. The plasma level of ABH

Table 2. *Epididymal fat pad weight/body weight*

	WT		WT-ABH		A1^{con}		EC-A1$^{-/-}$	
	ND	HFHS	ND	HFHS	ND	HFHS	ND	HFHS
EFPW/BW, %	3.50 ± 0.26	6.11 ± 0.26*	3.56 ± 0.22	5.92 ± 0.21*	3.7 ± 0.28	6.33 ± 0.24*	3.24 ± 0.42	5.96 ± 0.35*

Values are means ± SE; $n = 6$–8 mice. EFPW, epididymal fat pad weight; BW, body weight; ND, normal diet; HFHS, high fat-high sucrose diet; ABH, 2-(*S*)-amino-6-boronohexanoic acid; WT-ABH, wild-type mice treated with the arginase inhibitor ABH (10 mg·kg^{-1}·day^{-1} in drinking water); A1, arginase 1; ECs, endothelial cells; A1^{con}, control of knockout of A1 in ECs; EC-A1$^{-/-}$, A1 knockout-specific in ECs. *$P < 0.05$ vs. WT ND or A1^{con} ND groups.
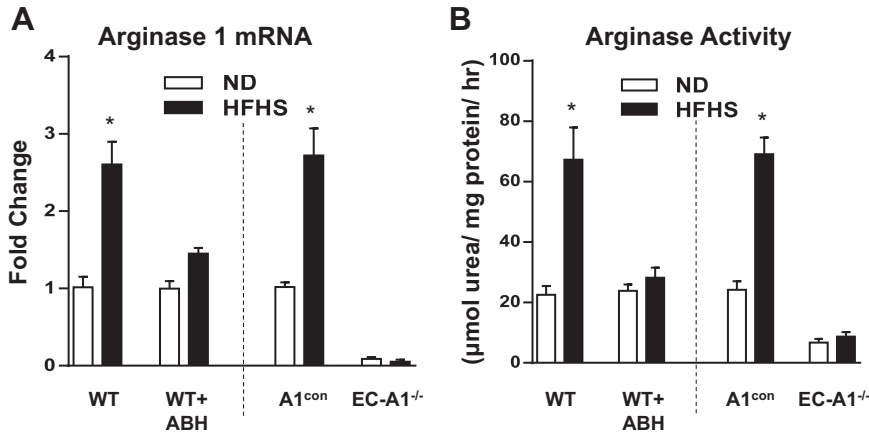
Fig. 1. Arginase inhibition or endothelial cell (EC)-arginase 1 (A1) deletion prevents high-fat/high-sucrose (HFHS)-induced increase in arginase activity and A1 mRNA expression in isolated aortic endothelial cells. Effects of 2-(S)-amino-6-boronohexanoic acid (ABH) and EC-A1 deletion on mRNA levels of A1 (A) and arginase activity (B). Values are means ± SE; $n = 6$ mice. *$P < 0.05$ vs. wild-type (WT) normal diet (ND) or A1con ND groups.

in WT mice on the ND was 0.27 ± 0.02 mmol/l after 5 mo of daily administration (see MATERIALS AND METHODS).

Our prior study showed that the HFHS diet induced an elevation of aortic arginase activity and expression of A1 in mice with intact EC-A1, but these effects were prevented in mice treated with ABH or lacking EC-A1 (4). Our present study shows a similar pattern of responses in aortic ECs isolated from mice in the same treatment groups. Arginase 1 mRNA and arginase activities were increased in ECs isolated from WT and A1con mice after HFHS diet feeding. Arginase 1 mRNA and arginase activity were not altered by the HFHS diet in ECs from mice treated with ABH or lacking EC-A1 (Fig. 1).

Effects of arginase inhibition or endothelial A1 deletion on expression of cytokines, chemokines, and adhesion molecules. Expression of cytokines and chemokines is critical for the activation and attraction of immune cells to sites of inflammation (1). After 6 mo of HFHS feeding, protein or mRNA levels of the proinflammatory cytokine TNF-α and the chemokine MCP-1 were significantly increased in ECs isolated from aorta (Fig. 2, A and B) and SVF of VAT (Fig. 3, A and B) from wild-type and genetic control (A1con) mice, as compared with mice fed the ND. HFHS diet also raised protein or mRNA levels for the anti-inflammatory cytokine IL-10, commonly induced in response to inflammation, in isolated ECs (Fig. 2C)
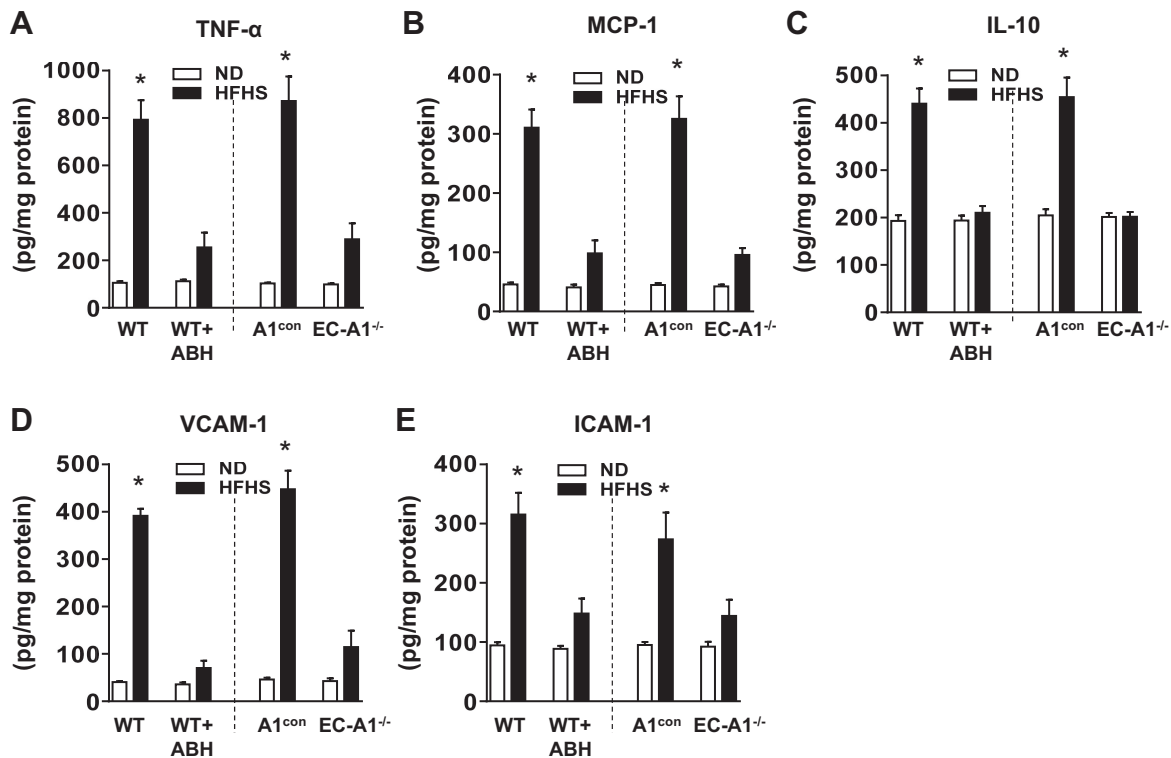

Fig. 2. Arginase inhibition or EC-A1 deletion prevents HFHS-induced increased in expression of cytokines, chemokines and adhesion molecules in isolated aortic endothelial cells. Effects of ABH and EC-A1 deletion on protein levels of the proinflammatory cytokine tumor necrosis factor-α (TNF-α; A), the chemokine monocyte chemoattractant protein-1 (MCP-1; B), anti-inflammatory interleutin-10 (IL-10; C), adhesion molecules vascular cell adhesion molecule-1 (VCAM-1; D), and intercellular adhesion molecule 1 (ICAM; E). Values are means ± SE; $n = 6$ mice. *$P < 0.05$ vs. WT ND or A1con ND groups.
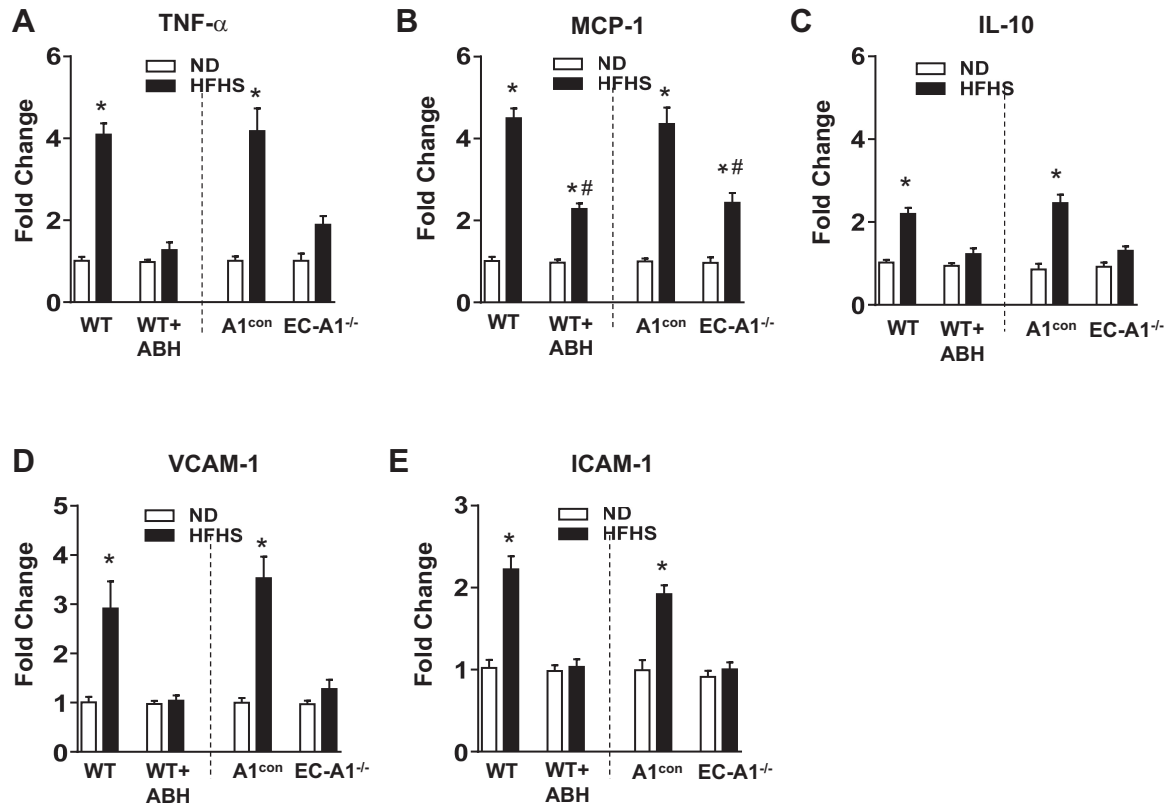
Fig. 3. Arginase inhibition or EC-A1 deletion prevents HFHS-induced increased in expression of cytokines, chemokines, and adhesion molecules in stromal vascular fraction of adipose tissues. Effects of ABH and EC-A1 deletion on mRNA levels of the proinflammatory cytokine TNFα-(A), the chemokine MCP-1 (B), the anti-inflammatory IL-10 (C), and adhesion molecules VCAM-1 (D) and ICAM-1 (E). Values are means ± SE; $n = 8$ mice. *$P < 0.05$ vs. WT ND or A1^{con} ND groups. #$P < 0.05$, WT HFHS + ABH or A1$^{-/-}$ HFHS vs. WT HFHS or A1^{con} HFHS groups, respectively.

and SVF (Fig. 3C). Treatment with ABH or deletion of A1 in vascular ECs blocked or partially prevented all of these elevations.

Expression of vascular adhesion molecules is necessary for monocyte attachment to the vascular endothelium and infiltration into the surrounding tissue (8). Both protein or mRNA levels for VCAM-1 and ICAM-1 were significantly increased in isolated ECs (Fig. 2, D and E) or SVF (Fig. 3, D and E) from HFHS treated WT and A1^{con} mice, respectively. The HFHS-induced increases in VCAM-1 and ICAM-1 protein and mRNA expression were all largely prevented by ABH treatment or by A1 deletion in ECs. Protein and mRNA levels of these vascular adhesion molecules and cytokines were not altered in the aortic ECs, VAT, or SVF of mice on the ND given ABH or lacking EC-A1 (Figs. 2 and 3).

Effects of arginase inhibition or A1 deletion in ECs on circulating inflammatory monocytes and macrophage infiltration. An increase in the levels of circulating, activated monocytes is also an indicator of vascular inflammation (53). To evaluate this inflammatory response in HFHS mice, we used flow cytometry to determine the percentage of circulating white cells with high levels of Ly6C. Ly6C is a glycoprotein expressed mainly in monocytes and can be used to distinguish between inflammatory monocytes (Ly6C^{high}) and patrolling monocytes (Ly6C^{low}). During inflammation, Ly6C^{high} monocytes are preferentially recruited into the inflamed tissue, where the majority mature as inflammatory M1-like macrophages (49).The percentage of Ly6C^{high} inflammatory mono-

cytes was significantly increased in the blood of HFHS treated WT and A1^{con} mice (Fig. 4, A–D). This elevation in inflammatory monocytes was prevented by ABH treatment or by deletion of A1 in ECs.

To determine the effect of HFHS on the accumulation of monocytes/macrophages in the VAT, we used flow cytometry to determine the percentage of macrophages (F4/80^{high} cells) within the SVF. In HFHS-fed WT and A1^{con} mice, the number of macrophages in the SVF was markedly increased above levels in ND mice (Fig. 4, E–H). ABH treatment or deletion of endothelial A1 largely prevented this rise.

We further examined the phenotypes of the SVF cells with antibodies against the integrin CD11c and the mannose receptor CD206. CD11c is highly expressed in proinflammatory M1-like macrophages, whereas CD206 is highly expressed in anti-inflammatory M2-like macrophages (13, 23). HFHS diet caused a five- to sixfold increase in the percentage of M1-like macrophage as compared with ND WT and A1^{con} control mice (Fig. 5, A, B, D, and E). On the other hand, HFHS feeding caused a similar reduction in the percentage of M2-like macrophage (Fig. 5, A, C, D, and F). These alterations were partially blocked by ABH treatment or deletion of A1 in ECs. These results suggest that arginase activity and A1 expression in ECs play a major role in inflammatory reactions in both vascular and adipose tissue.

Effects of HFHS diet on adipocyte size, collagen deposition, and capillary density in VAT. As stated earlier, obesity-induced inflammation is thought to result from pathological expansion
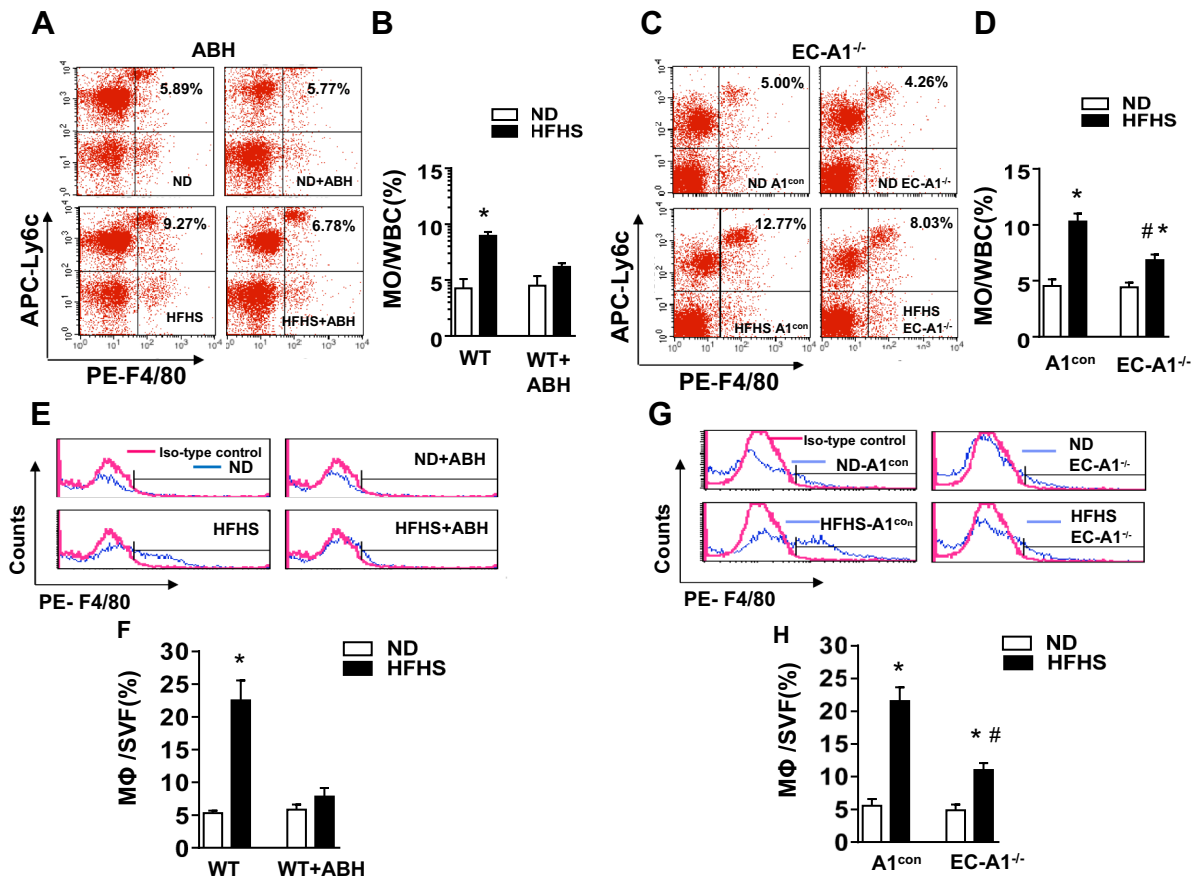
Fig. 4. Arginase inhibition or EC-A1 deletion prevents or blunts the HFHS-induced increases in circulating inflammatory monocytes and limits macrophage infiltration into stromal vascular fraction of visceral adipose tissue. Representative FACS profile showing effects of ABH (*A*) or EC-A1 deletion (*C*) on the percentage of circulating white blood cells (WBC) with high levels of both Ly6C and F4/80. APC, allophycocyanin; PE, phycoerythrin. Histograms show the percentage of Ly6C^{high}/F4/80^{high} inflammatory monocytes (MO) in total circulating blood cells (*B* and *D*). Representative FACS profile showing effects of ABH (*E*) or EC-A1 deletion (*G*) on percentage of macrophages (F4/80^{high}) within the stromal vascular fraction (SVF). Histograms show the percentage of macrophage (MΦ) cells in the SVF (*F* and *H*). Values are means ± SE; $n = 5$–7 mice. *$P < 0.05$ vs. WT ND or A1^{con} ND groups. #$P < 0.05$ vs. WT HFHS or A1^{con} HFHS groups.

and fibrosis of the VAT in a context of vascular rarefaction and reduced blood flow, leading to hypoxia, adipocyte death, and activation of resident immune cells, which release inflammatory mediators. Our morphometric analysis of VAT showed that in A1^{con} mice, the HFHS diet caused adipocyte hypertrophy, collagen deposition/fibrosis, and macrophage infiltration with formation of "crown-like" structures around the degenerating adipocytes, along with decreased capillary density (Fig. 6, *A*–*C*) versus ND controls. These effects of HFHS were prevented or blunted in mice lacking EC-A1 (Fig. 6*D*).

Effects of high-glucose/palmitate treatment on arginase expression/activity and NO production and inflammatory reactions in ECs. We examined potential mechanisms underlying the effects of HFHS diet-induced increases in arginase activity, A1 expression, NO production, and inflammatory reactions in vascular ECs by studies using MAECs maintained for 48 h in media containing 25 mM glucose and 200 μM palmitate (HG + PA). To assess the specific role of A1 in HG + PA-induced alterations, we used CRISPR/Cas 9-transduction of sgRNA to reduce A1 expression.

The HG + PA treatment increased levels of A1 mRNA and protein expression in normal and vector-transduced MAECs

(Fig. 7, *A*–*C*). These elevations were not altered by ABH treatment (Fig. 7, *A* and *B*). However, A1 sgRNA transfection significantly inhibited the HG + PA-induced increase in A1 mRNA and protein expression compared with the vector transfection group. (Fig. 7, *A* and *C*). Arginase activity was also significantly increased by HG + PA treatment (Fig. 7*D*). This increase in arginase activity was accompanied by a marked decrease in NO production (Fig. 7*E*). Both ABH and A1-sgRNA transfection significantly blocked the HG + PA-induced increase in arginase activity (Fig. 7*D*).

Consistent with the decrease in arginase activity, both ABH and A1 knockdown prevented the HG + PA-induced reduction in NO production (Fig. 7*E*). Treatment with the NOS inhibitor L-NAME (100 μM) prevented the protective effect of ABH and A1 knockdown in maintaining production of NO in cells exposed to HG + PA (Fig. 7*E*). In control cultures, L-NAME reduced NO production levels by ~90% (from 18.3 ± 1.9 to 2.0 ± 0.3 pM, control vs. control + L-NAME). The higher NO levels in cultures exposed to high-glucose/palmitate + L-NAME are likely due to elevated inducible NOS (NOS-2), which is induced by inflammatory cytokines and far less sensitive to L-NAME than endothelial NOS (40).
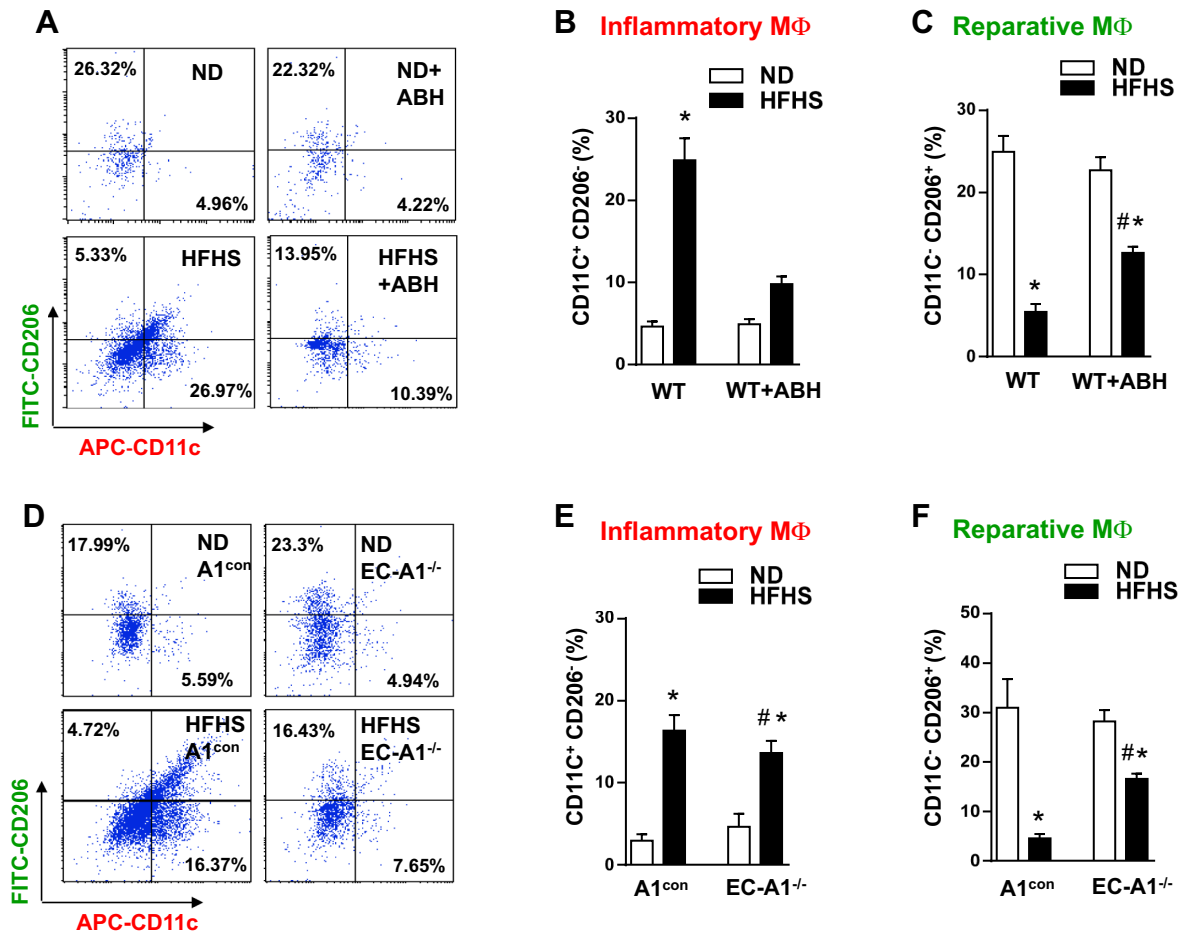
Fig. 5. Arginase inhibition or EC-A1 deletion blunts the HFHS-induced increases in proinflammatory macrophages and limits the HFHS-induced decreases in reparative macrophages in visceral adipose tissue. Representative FACS profile showing effects of ABH (*A*) or EC-A1 deletion (*D*) on the percentage of proinflammatory (M1-like) macrophages (CD11C^{high}, CD206^{low}, and F4/80^{high}) and reparative (M2-like) macrophages (CD11C^{low}, CD206^{high}, and F4/80^{high}) to total macrophages (F4/80^{high}) in SVF. Flow plots correspond to the F4/80 gate. Histograms show effects of ABH (*B* and *C*) or EC-A1 deletion (*E* and *F*) on the proportions of proinflammatory and reparative macrophages to total macrophages. Values are means $\pm$ SE; $n = 5$–7 mice. *$P < 0.05$ vs. WT ND or A1^{con} ND groups. #$P < 0.05$ vs. WT HFHS or A1^{con} HFHS groups.

We also examined the effects of the HG + PA treatment on EC inflammatory reactions as shown by expression of vascular adhesion molecules, chemokines, and cytokines and whether the inhibition of arginase activity or A1 knockdown can prevent this activation by regulating NO production. Quantitative RT-PCR analysis showed that HG + PA treatment increased levels of mRNA for ICAM-1, VCAM-1, and MCP-1 compared with normal control media (Table 3). ABH treatment or A1 knockdown prevented or blunted all of these increases. Pretreatment with L-NAME (100 μM) blocked these protective effects of ABH treatment or A1 knockdown, demonstrating the critical role of NOS activity in producing NO in limiting activation of EC inflammation. The mRNA levels of the proinflammatory cytokine TNFα and the anti-inflammatory cytokine IL-10 also were significantly increased by HG + PA treatment as compared with normal control media. However, neither arginase inhibition nor A1 knockdown altered this rise (Table 4).

Adhesion of circulating monocytes to ECs is a critical step in early stages of inflammation and macrophage infiltration. To assess the roles of arginase activity and A1 expression in this process, we added cultured monocytes to ECs maintained in HG + PA or control media. Our analysis showed that, consistent with the HG + PA-induced expression of vascular adhesion molecules, monocyte adhesion to HG + PA-treated ECs also was increased compared with cells maintained in the normal media (Fig. 8). This increased monocyte adhesion was blocked by either ABH treatment or A1-sgRNA transfection of MAECs. Moreover, cotreatment with L-NAME prevented these protective effects, suggesting that the HG + PA-induced monocyte EC adhesion is mediated by the action of A1 in decreasing NO production.

DISCUSSION

Increasing evidence indicates that conditions of obesity and type 2 diabetes are highly associated with a chronic inflammatory response characterized by high levels of circulating proinflammatory cytokines and fatty acids and vascular inflammation (3, 38). Downregulation of vascular NO production and excessive ROS formation are considered prime factors in the process of vascular inflammation and dysfunction (18). Previous studies have reported that elevation of arginase activity is highly associated with this imbalance in vascular NO and ROS levels (37). Our recent studies of HFHS diet-fed mice have further demonstrated that deletion of A1 in vascular ECs or
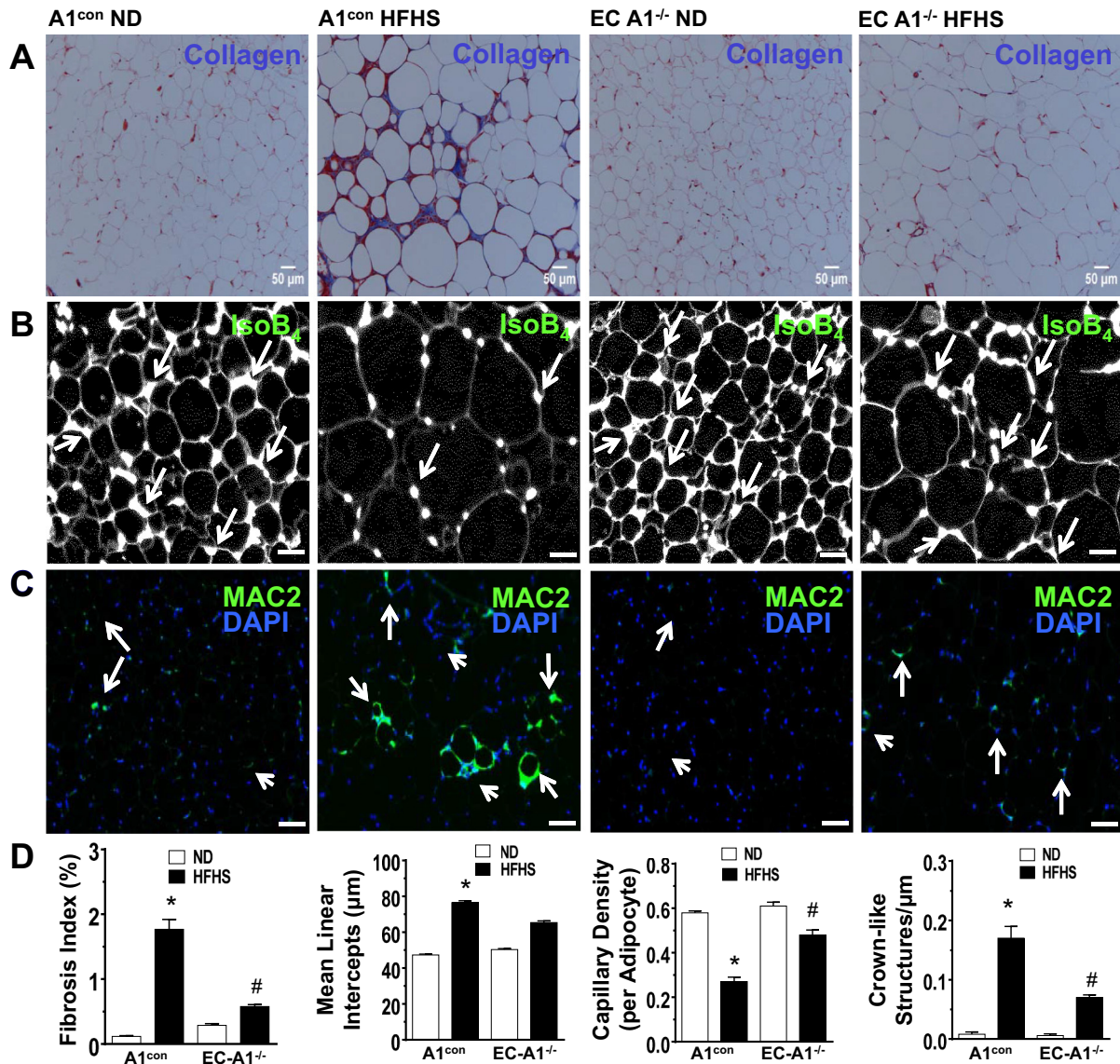
Fig. 6. Masson's trichrome, isolectin B4, and Mac2 staining of paraffin-embedded visceral adipose tissue sections. Representative photomicrographs show Masson's trichrome staining [collagen/fibrosis (blue color) and adipocyte size; *A*], isolectin B4 stain (capillary density, green color; *B*), and MAC2 antibody stain [macrophage/crown-like structures (CLS; green-blue; *C*)] in visceral adipose tissue (VAT) sections from A1^{con} and EC-A1-deficient mice fed ND or HFHS diet. Histograms show results of quantitative analysis of collagen/fibrosis, adipocyte size, capillary density, and crown-like structures (*D*); $n = 5$–6 experiments. *$P < 0.01$ vs. A1^{con} HFHS group. #$P < 0.01$ vs. A1$^{-/-}$ HFHS group.

arginase inhibitor treatment effectively prevents vascular endothelial dysfunction by reducing ROS and maintaining levels of NO (4). In the present report, we demonstrate for the first time the key role of arginase activity and endothelial A1 expression in HFHS diet-induced inflammation and pathological remodeling of the VAT.

During the progression of inflammation, the activated vascular endothelium responds to the compromised circulation by recruiting circulating monocytes through increased release of the chemoattractant protein MCP-1 and upregulation of adhesion proteins ICAM-1 and VCAM-1 on its luminal surface. This induces leukocyte attraction, attachment to the vessel wall, and transmigration into the underlying tissue (8, 10, 16). An important mechanism involved in HFHS diet-induced vascular inflammation and vasculopathy is reduced NO levels. A recent study has shown the involvement of NADPH oxidase, ROS, and TNF-α in the reduction of NO levels in mice fed a similar HFHS diet (34). NO has integral roles in limiting many aspects of inflammatory responses. Endothelial NO prevents activation of the endothelium and thus reduces the adhesion, infiltration, and transmigration of circulating inflammatory immune cells into the vascular wall (41). Both EC-derived NO and NO donors have been shown to inhibit endothelial expression of MCP-1, ICAM-1, and VCAM-1 (11, 51). Our present findings support these reports on the role of NO is suppressing this inflammatory process.

Our study also found that the HFHS-induced increases in VCAM-1, ICAM-1, and MCP-1 expression in both vascular ECs and VAT were accompanied by elevated arginase activity and A1 expression in vascular ECs. These increases in inflammatory mediators were all blunted by ABH or lack of A1 in ECs, indicating involvement of vascular arginase in this pa-
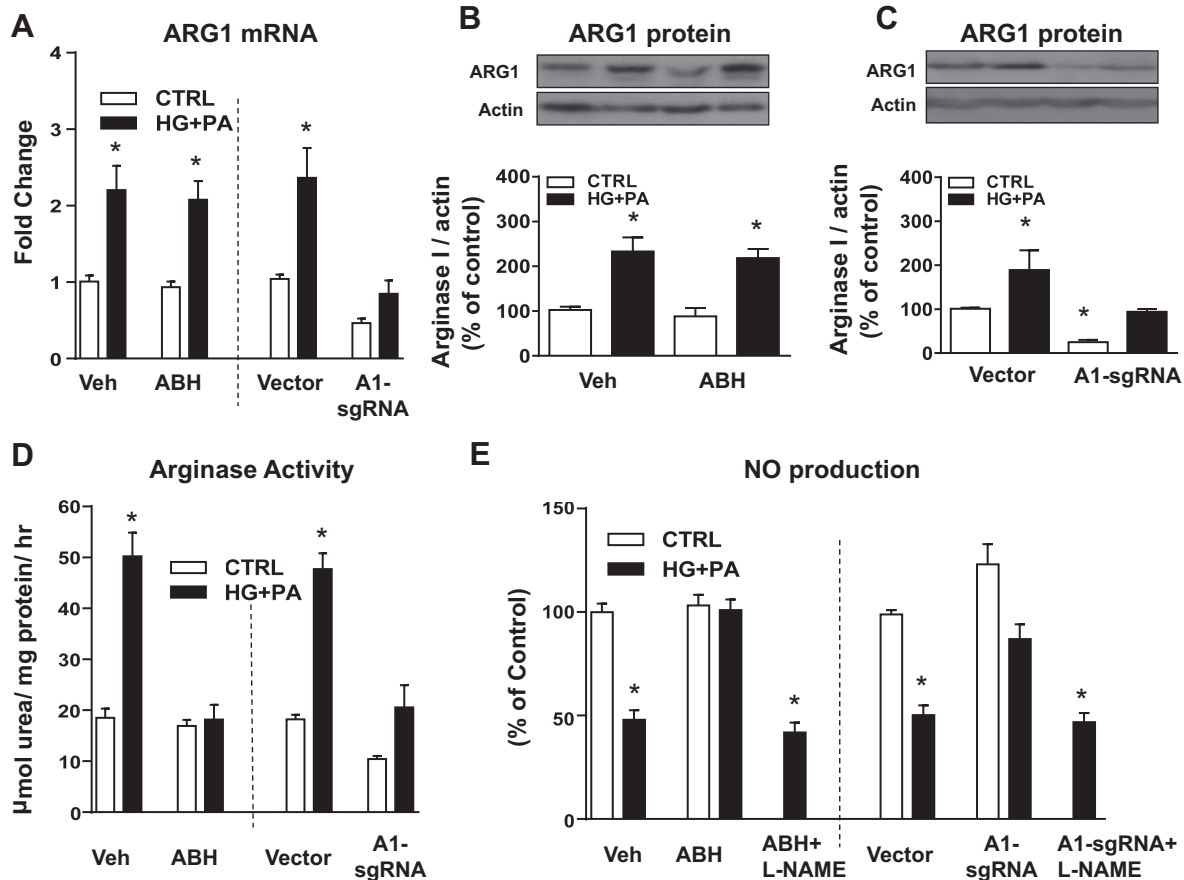
Fig. 7. Effects of arginase inhibitor or A1 knockdown on A1 expression/activity and nitric oxide (NO) production in HG + PA-incubated endothelial cells. A1 mRNA (A) and protein expression (B and C) and arginase activity (D) with arginase inhibitor treatment and A1 knockdown by CRISPR/Cas 9-transduction of sgRNA with a 48-h exposure to normal control media (CTRL) or media with high glucose (HG; 25 mM) and palmitate (PA; 200 µM). NO production with and without ABH and nitric oxide synthase inhibitor [nitro-L-arginine methyl ester (L-NAME)] treatment and A1 downregulation with 48-h exposure to CTRL or HG + PA media (E). Values are means ± SE; $n = 4–6$ experiments. *$P < 0.05$ vs. vehicle-treated (Veh) cells or vector-transfected cells in control media.

thology. The dominant role of endothelial NOS function in controlling vascular inflammation may explain why the specific deletion of the endothelial A1 gene is so effective in limiting HFHS-induced inflammation.

Circulating inflammatory monocytes with high levels of the Ly6C (Ly6C^{high}) are preferentially recruited to inflamed tissue and are considered to be more likely to mature as an M1-like macrophage. The release of these LyC6^{high} monocytes from bone marrow can be enhanced by chemokines emanating from inflamed tissue and by their increased egress across the activated bone marrow capillary endothelium (39, 49). We observed that the HFHS diet substantially increased levels of

these monocytes and that arginase activity and endothelial A1 are involved in this inflammatory process.

Macrophage infiltration into adipose tissue and release of proinflammatory cytokines such as TNFα are integral to obesity-related inflammation (14, 25, 45, 48). In obesity and diabetes, adipose tissue is infiltrated with large numbers of macrophages, which can comprise up to 40% of the cells within adipose tissue (45, 48). The inflammatory (M1-like) macrophage is the predominant phenotype in obesity-induced inflammation of the VAT (26, 30). Our study showed marked infiltration of M1-like macrophage along with increased levels of TNF-α mRNA in the VAT of HFHS-fed mice. This was associated with

Table 3. *Fold changes in mRNA of chemokines and adhesion molecules in mouse aortic endothelial cells*

	Veh		ABH		ABH + L-NAME	Vector		A1-sgRNA		A1-sgRNA + L-NAME
	CTRL	HG + PA	CTRL	HG + PA		CTRL	HG + PA	CTRL	HG + PA	
MCP-1	1.03 ± 0.05	4.96 ± 0.54*	0.97 ± 0.03	1.87 ± 0.23*#	3.03 ± 0.39*	1.02 ± 0.08	5.04 ± 0.56*	0.63 ± 0.21	1.89 ± 0.26*#	3.13 ± 0.48*
ICAM-1	1.03 ± 0.08	5.00 ± 0.58*	1.05 ± 0.13	1.26 ± 0.21	3.48 ± 0.46*	1.04 ± 0.20	4.18 ± 0.66*	1.00 ± 0.11	1.40 ± 0.19	3.01 ± 0.51*
VCAM-1	1.07 ± 0.11	11.74 ± 2.71*	1.18 ± 0.13	1.90 ± 0.47	10.95 ± 2.03*	1.05 ± 0.15	12.14 ± 2.57*	1.13 ± 0.14	1.94 ± 0.42	9.66 ± 2.02*

Values are means ± SE; $n = 5$ experiments. mRNA levels of MCP-1, ICAM-1, and V-CAM-1 in mouse aortic endothelial cells (MAECs) with and without arginase inhibitor (ABH), nitric oxide synthase inhibitor [nitro-L-arginine methyl ester (L-NAME)] treatment, or A1 downregulation by CRISPR/Cas 9-transduction of sgRNA after a 48-h incubation in normal media (CTRL) or media containing high glucose and palmitate (HG + PA). *$P < 0.05$ vs. CTRL vehicle or vector-transfected groups. #$P < 0.05$ HG + PA + ABH or A1-sgRNA HG + PA vs. Veh HG + PA or vector-transfected HG + PA groups, respectively.

Table 4. *mRNA fold changes of cytokines in mouse aorta endothelial cells*

	Veh		ABH		Vector		A1-sgRNA	
	CTRL	HG + PA	CTRL	HG + PA	CTRL	HG + PA	CTRL	HG + PA
TNF-α	1.02 ± 0.10	13.9 ± 1.89*	1.17 ± 0.36	14.9 ± 1.31*	1.03 ± 0.10	13.3 ± 2.46*	0.95 ± 0.11	11.80 ± 2.28*
IL-10	1.01 ± 0.12	1.66 ± 0.05*	0.99 ± 0.15	1.58 ± 0.15*	1.02 ± 0.17	1.72 ± 0.09*	1.08 ± 0.21	1.77 ± 0.13*

Values are means ± SE; $n = 5$ experiments. mRNA levels of TNF-α and IL-10 in MAECs with and without arginase inhibitor (ABH) or ARG1 knockdown by CRISPR/Cas 9 transduction of sgRNA after 48 h incubation in normal media (CTRL) or media containing high glucose and palmitate (HG + PA). *$P < 0.05$ vs. CTRL vehicle or vector-transfected groups.

a reduction in the M2-like macrophages. Inhibition of arginase or lack of endothelial A1 markedly reduced these alterations, underscoring the role of EC-A1 in the pathological process.

The HFHS diet-induced increases in macrophage activation and infiltration of the VAT were accompanied by signs of pathological remodeling, including adipocyte hypertrophy, increased collagen deposition/fibrosis, decreased capillary density, and formation of numerous "crown-like" structures comprised of macrophages surrounding degenerating adipocytes. These alterations were prevented or significantly inhibited by deletion of A1 in the vascular ECs, further supporting the specific involvement of endothelial A1 in the pathology.

Our experiments with cultured mouse aortic ECs maintained in high-glucose-palmitate media confirmed the critical role of EC expression of A1 in limiting NO production and inducing EC activation and monocyte attachment. Downregulation of A1 expression and activity with sgRNA markly improved NO production; decreased MCP-1, ICAM-1, and VCAM-1 expres-

sion; and inhibited monocyte adhesion in cells exposed to the high-glucose-palmitate media. Treatment with the NOS inhibitor L-NAME effectively prevented each of the beneficial effects. These observations indicate that the anti-inflammatory and antiadhesive effects of arginase inhibition and A1 knockdown are mediated through maintenance of endothelial NO levels, via a reduction in arginase activity.

In closing, HFHS diet-induced obesity and type 2 diabetes in mice is characterized by endothelial activation, vascular inflammation, and increased levels of circulating inflammatory monocytes along with VAT fibrosis, vascular rarefaction, and increased infiltration by inflammatory M1-like macrophage. Inhibition of arginase or deletion of endothelial A1 prevented or markedly reduced these changes. ECs exposed to high glucose and palmitate exhibited an inflammatory phenotype and impaired NO synthesis that were prevented by arginase inhibition of A1 downregulation. These findings imply a primary role for EC-A1 in obesity-induced inflammation and VAT dysfunction.
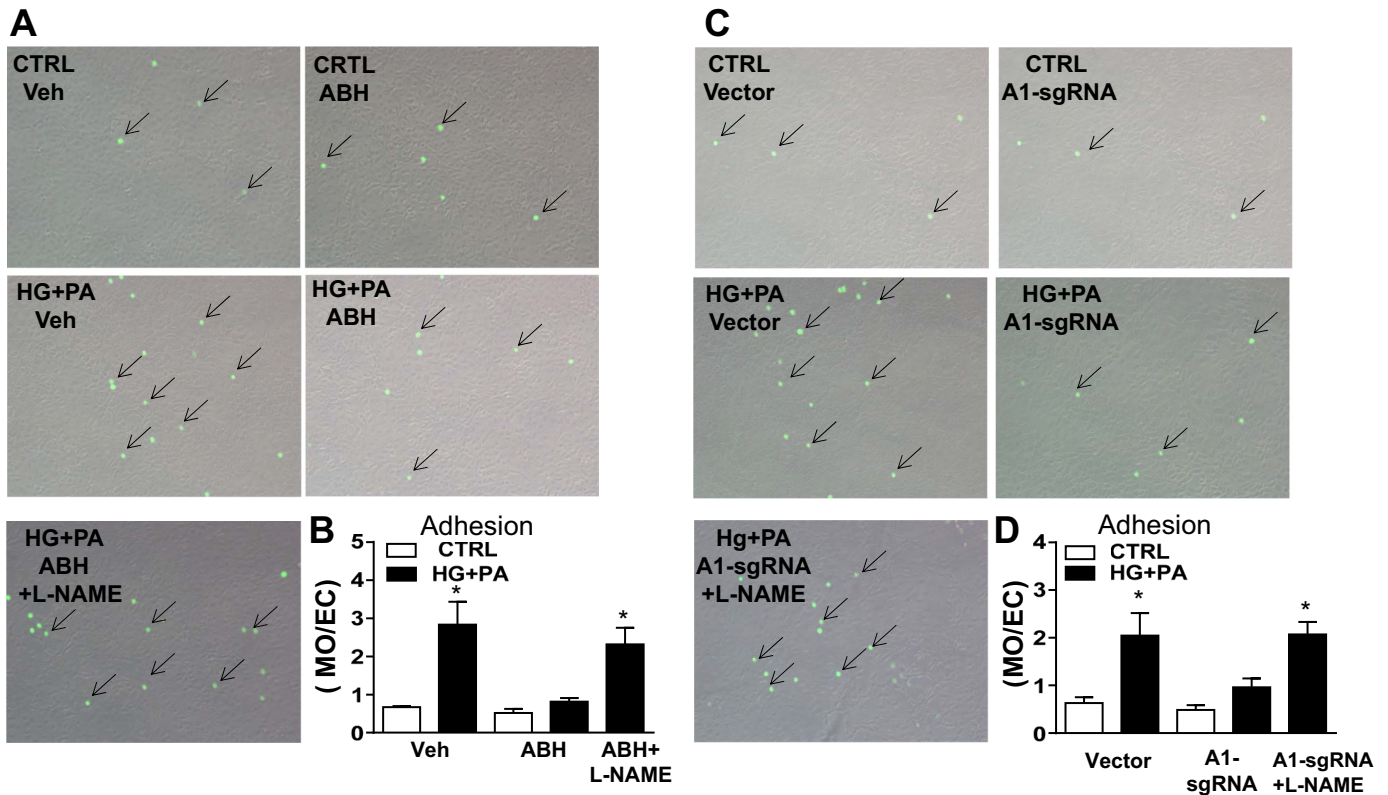

Fig. 8. Effects of arginase inhibition or A1 knockdown on monocyte attachment to HG + PA incubated cells. Representative images showing monocyte (calcein AM stain, arrows) attachment to the HG + PA treated endothelial cells vs. cells maintained in normal media (CTRL) or treated with arginase inhibitor, nitric oxide synthase inhibitor (L-NAME), or CRISPR/Cas 9-transduction of sgRNA to knockdown A1 (*A* and *C*). Histograms show the relative numbers of calcein AM stained monocytes attached/endothelial cell among the groups (*B* and *D*). Values are means ± SE; $n = 4–5$ experiments. *$P < 0.05$ vs. CTRL cells.

Perspectives and Significance

Storage of fat in adipose tissue is an extremely important protective source of energy to prevent or delay starvation when food is unavailable. However, as levels of physical activity have fallen and abundance of food has risen in many cultures, obesity and type 2 diabetes have become a growing global health problem. According to the World Health Organization, in 2014 ~600 million people worldwide were chronically obese and many had type 2 diabetes; the GBD 2015 Obesity Collaborators reported an even greater prevalence (13a, 47). The prevailing hypothesis in the field is that obesity-induced metabolic disease and cardiovascular dysfunction are secondary to inflammation and pathological remodeling of VAT in the context of vascular rarefaction and limited blood flow, adipocyte death, and immune cell activation (29). Obesity-induced type 2 diabetes has been increasingly recognized as an inflammatory disease, involving high circulating and tissue levels of proinflammatory cytokines and fatty acids (43). Our current results support the hypothesis that VAT dysfunction is driven by an A1-mediated vascular endothelial dysfunction, which subsequently leads to enhanced VAT inflammation, fibrosis, and related vascular pathologies. It should be noted, however, that since systemic inhibition of arginase is generally more effective than EC-A1 deletion in preventing these pathologies, arginase in other cells is also likely to be involved.

DISCLOSURES

No conflicts of interest, financial or otherwise, are declared by the authors.

AUTHOR CONTRIBUTIONS

L.Y., A.B., R.B.C., and R.W.C. conceived and designed research; L.Y., A.B., Z.X., J.C., H.A.T., Y.C., Z.B., and Y.H. performed experiments; L.Y., A.B., Z.X., J.C., H.A.T., Y.C., Y.X., Z.B., R.L., Y.H., R.B.C., and R.W.C. analyzed data; L.Y., A.B., Z.X., J.C., H.A.T., Y.X., and Z.B. prepared figures; L.Y., A.B., and R.B.C. drafted manuscript; L.Y., A.B., Z.B., R.L., Y.H., R.B.C., and R.W.C. edited and revised manuscript; Y.X., Z.B., R.L., Y.H., R.B.C., and R.W.C. interpreted results of experiments; R.W.C. and L.Y. approved final version of manuscript.

REFERENCES

1. **Arango Duque G, Descoteaux A.** Macrophage cytokines: involvement in immunity and infectious diseases. *Front Immunol* 5: 491, 2014. doi:10.3389/fimmu.2014.00491.

2. **Beleznai T, Feher A, Spielvogel D, Lansman SL, Bagi Z.** Arginase 1 contributes to diminished coronary arteriolar dilation in patients with diabetes. *Am J Physiol Heart Circ Physiol* 300: H777–H783, 2011. doi:10.1152/ajpheart.00831.2010.

3. **Berg AH, Scherer PE.** Adipose tissue, inflammation, and cardiovascular disease. *Circ Res* 96: 939–949, 2005. doi:10.1161/01.RES.0000163635.62927.34.

4. **Bhatta A, Yao L, Xu Z, Chen J, Toque HA, Atawia R, Fouda A, Bagi Z, Lucas R, Caldwell RB, Caldwell RW.** Obesity-induced vascular dysfunction and vascular stiffening require endothelial cell arginase. *Cardiovasc Res.* 7 Sept 2017. doi:10.1093/cvr/cvx164.

5. **Caldwell RB, Toque HA, Narayanan SP, Caldwell RW.** Arginase: an old enzyme with new tricks. *Trends Pharmacol Sci* 36: 395–405, 2015. doi:10.1016/j.tips.2015.03.006.

6. **Chandra S, Romero MJ, Shatanawi A, Alkilany AM, Caldwell RB, Caldwell RW.** Oxidative species increase arginase activity in endothelial cells through the RhoA/Rho kinase pathway. *Br J Pharmacol* 165: 506–519, 2012. doi:10.1111/j.1476-5381.2011.01584.x.

8. **Collins RG, Velji R, Guevara NV, Hicks MJ, Chan L, Beaudet AL.** P-Selectin or intercellular adhesion molecule (ICAM)-1 deficiency substantially protects against atherosclerosis in apolipoprotein E-deficient mice. *J Exp Med* 191: 189–194, 2000. doi:10.1084/jem.191.1.189.

9. **Corraliza IM, Campo ML, Soler G, Modolell M.** Determination of arginase activity in macrophages: a micromethod. *J Immunol Methods* 174: 231–235, 1994. doi:10.1016/0022-1759(94)90027-2.

10. **Dansky HM, Barlow CB, Lominska C, Sikes JL, Kao C, Weinsaft J, Cybulsky MI, Smith JD.** Adhesion of monocytes to arterial endothelium and initiation of atherosclerosis are critically dependent on vascular cell adhesion molecule-1 gene dosage. *Arterioscler Thromb Vasc Biol* 21: 1662–1667, 2001. doi:10.1161/hq1001.096625.

11. **De Caterina R, Libby P, Peng HB, Thannickal VJ, Rajavashisth TB, Gimbrone MA Jr, Shin WS, Liao JK.** Nitric oxide decreases cytokine-induced endothelial activation. Nitric oxide selectively reduces endothelial expression of adhesion molecules and proinflammatory cytokines. *J Clin Invest* 96: 60–68, 1995. doi:10.1172/JCI118074.

12. **Dunay IR, Fuchs A, Sibley LD.** Inflammatory monocytes but not neutrophils are necessary to control infection with Toxoplasma gondii in mice. *Infect Immun* 78: 1564–1570, 2010. doi:10.1128/IAI.00472-09.

13. **Fujisaka S, Usui I, Bukhari A, Ikutani M, Oya T, Kanatani Y, Tsuneyama K, Nagai Y, Takatsu K, Urakaze M, Kobayashi M, Tobe K.** Regulatory mechanisms for adipose tissue M1 and M2 macrophages in diet-induced obese mice. *Diabetes* 58: 2574–2582, 2009. doi:10.2337/db08-1475.

13a. **GBD 2015 Obesity Collaborators; Afshin A, Forouzanfar MH, Reitsma MB, Sur P, Estep K, Lee A, Marczak L, Mokdad AH, Moradi-Lakeh M, Naghavi M, Salama JS, Vos T, Abate KH, Abbafati C, Ahmed MB, Al-Aly Z, Alkerwi A, Al-Raddadi R, Amare AT, Amberbir A, Amegah AK, Amini E, Amrock SM, Anjana RM, Ärnlöv J, Asayesh H, Banerjee A, Barac A, Baye E, Bennett DA, Beyene AS, Biadgilign S, Biryukov S, Bjertness E, Boneya DJ, Campos-Nonato I, Carrero JJ, Cecilio P, Cercy K, Ciobanu LG, Cornaby L, Damtew SA, Dandona L, Dandona R, Dharmaratne SD, Duncan BB, Eshrati B, Esteghamati A, Feigin VL, Fernandes JC, Fürst T, Gebrehiwot TT, Gold A, Gona PN, Goto A, Habtewold TD, Hadush KT, Hafezi-Nejad N, Hay SI, Horino M, Islami F, Kamal R, Kasaeian A, Katikireddi SV, Kengne AP, Kesavachandran CN, Khader YS, Khang YH, Khubchandani J, Kim D, Kim YJ, Kinfu Y, Kosen S, Ku T, Defo BK, Kumar GA, Larson HJ, Leinsalu M, Liang X, Lim SS, Liu P, Lopez AD, Lozano R, Majeed A, Malekzadeh R, Malta DC, Mazidi M, McAlinden C, McGarvey ST, Mengistu DT, Mensah GA, Mensink GB, Mezgebe HB, Mirrakhimov EM, Mueller UO, Noubiap JJ, Obermeyer CM, Ogbo FA, Owolabi MO, Patton GC, Pourmalek F, Qorbani M, Rafay A, Rai RK, Ranabhat CL, Reinig N, Safiri S, Salomon JA, Sanabria JR, Santos IS, Sartorius B, Sawhney M, Schmidhuber J, Schutte AE, Schmidt MI, Sepanlou SG, Shamsizadeh M, Sheikhbahaei S, Shin MJ, Shiri R, Shiue I, Roba HS, Silva DA, Silverberg JI, Singh JA, Stranges S, Swaminathan S, Tabarés-Seisdedos R, Tadese F, Tedla BA, Tegegne BS, Terkawi AS, Thakur JS, Tonelli M, Topor-Madry R, Tyrovolas S, Ukwaja KN, Uthman OA, Vaezghasemi M, Vasankari T, Vlassov VV, Vollset SE, Weiderpass E, Werdecker A, Wesana J, Westerman R, Yano Y, Yonemoto N, Yonga G, Zaidi Z, Zenebe ZM, Zipkin B, Murray CJ.** Health effects of overweight and obesity in 195 countries over 25 years. *N Engl J Med* 377: 13–27, 2017. doi:10.1056/NEJMoa1614362.

14. **Gormez S, Demirkan A, Atalar F, Caynak B, Erdim R, Sozer V, Gunay D, Akpinar B, Ozbek U, Buyukdevrim AS.** Adipose tissue gene expression of adiponectin, tumor necrosis factor-α and leptin in metabolic

syndrome patients with coronary artery disease. *Intern Med* 50: 805–810, 2011. doi:10.2169/internalmedicine.50.4753.

15. **Gross ML, Heiss N, Weckbach M, Hansen A, El-Shakmak A, Szabo A, Münter K, Ritz E, Amann K.** ACE-inhibition is superior to endothelin A receptor blockade in preventing abnormal capillary supply and fibrosis of the heart in experimental diabetes. *Diabetologia* 47: 316–324, 2004. doi:10.1007/s00125-003-1309-z.

16. **Gu L, Okada Y, Clinton SK, Gerard C, Sukhova GK, Libby P, Rollins BJ.** Absence of monocyte chemoattractant protein-1 reduces atherosclerosis in low density lipoprotein receptor-deficient mice. *Mol Cell* 2: 275–281, 1998. doi:10.1016/S1097-2765(00)80139-2.

17. **Hu H, Moon J, Chung JH, Kim OY, Yu R, Shin MJ.** Arginase inhibition ameliorates adipose tissue inflammation in mice with diet-induced obesity. *Biochem Biophys Res Commun* 464: 840–847, 2015. doi:10.1016/j.bbrc.2015.07.048.

18. **Iwata NG, Pham M, Rizzo NO, Cheng AM, Maloney E, Kim F.** Trans fatty acids induce vascular inflammation and reduce vascular nitric oxide production in endothelial cells. *PLoS One* 6: e29600, 2011. doi:10.1371/journal.pone.0029600.

19. **Johnson FK, Peyton KJ, Liu XM, Azam MA, Shebib AR, Johnson RA, Durante W.** Arginase promotes endothelial dysfunction and hypertension in obese rats. *Obesity (Silver Spring)* 23: 383–390, 2015. doi:10.1002/oby.20969.

20. **Jung C, Quitter F, Lichtenauer M, Fritzenwanger M, Pfeil A, Shemyakin A, Franz M, Figulla HR, Pfeifer R, Pernow J.** Increased arginase levels contribute to impaired perfusion after cardiopulmonary resuscitation. *Eur J Clin Invest* 44: 965–971, 2014. doi:10.1111/eci.12330.

21. **Laakso M.** Diabetes as a "cardiovascular disease equivalent": implications for treatment. *Nat Clin Pract Cardiovasc Med* 5: 682–683, 2008. doi:10.1038/ncpcardio1344.

22. **Llauradó G, Ceperuelo-Mallafré V, Vilardell C, Simó R, Freixenet N, Vendrell J, González-Clemente JM.** Arterial stiffness is increased in patients with type 1 diabetes without cardiovascular disease: a potential role of low-grade inflammation. *Diabetes Care* 35: 1083–1089, 2012. doi:10.2337/dc11-1475.

23. **Lumeng CN, Bodzin JL, Saltiel AR.** Obesity induces a phenotypic switch in adipose tissue macrophage polarization. *J Clin Invest* 117: 175–184, 2007. doi:10.1172/JCI29881.

24. **Makino A, Platoshyn O, Suarez J, Yuan JX, Dillmann WH.** Down-regulation of connexin40 is associated with coronary endothelial cell dysfunction in streptozotocin-induced diabetic mice. *Am J Physiol Cell Physiol* 295: C221–C230, 2008. doi:10.1152/ajpcell.00433.2007.

25. **Mazurek T, Zhang L, Zalewski A, Mannion JD, Diehl JT, Arafat H, Sarov-Blat L, O'Brien S, Keiper EA, Johnson AG, Martin J, Goldstein BJ, Shi Y.** Human epicardial adipose tissue is a source of inflammatory mediators. *Circulation* 108: 2460–2466, 2003. doi:10.1161/01.CIR.0000099542.57313.C5.

26. **Mestas J, Ley K.** Monocyte-endothelial cell interactions in the development of atherosclerosis. *Trends Cardiovasc Med* 18: 228–232, 2008. doi:10.1016/j.tcm.2008.11.004.

27. **Mills CD.** M1 and M2 macrophages: oracles of health and disease. *Crit Rev Immunol* 32: 463–488, 2012. doi:10.1615/CritRevImmunol.v32.i6.10.

28. **Münzel T, Daiber A, Ullrich V, Mülsch A.** Vascular consequences of endothelial nitric oxide synthase uncoupling for the activity and expression of the soluble guanylyl cyclase and the cGMP-dependent protein kinase. *Arterioscler Thromb Vasc Biol* 25: 1551–1557, 2005. doi:10.1161/01.ATV.0000168896.64927.bb.

29. **Nakamura K, Fuster JJ, Walsh K.** Adipokines: a link between obesity and cardiovascular disease. *J Cardiol* 63: 250–259, 2014. doi:10.1016/j.jjcc.2013.11.006.

30. **Odegaard JI, Chawla A.** Mechanisms of macrophage activation in obesity-induced insulin resistance. *Nat Clin Pract Endocrinol Metab* 4: 619–626, 2008. doi:10.1038/ncpendmet0976.

31. **Oltman CL, Richou LL, Davidson EP, Coppey LJ, Lund DD, Yorek MA.** Progression of coronary and mesenteric vascular dysfunction in Zucker obese and Zucker diabetic fatty rats. *Am J Physiol Heart Circ Physiol* 291: H1780–H1787, 2006. doi:10.1152/ajpheart.01297.2005.

32. **Pandey D, Bhunia A, Oh YJ, Chang F, Bergman Y, Kim JH, Serbo J, Boronina TN, Cole RN, Van Eyk J, Remaley AT, Berkowitz DE, Romer LH.** OxLDL triggers retrograde translocation of arginase2 in aortic endothelial cells via ROCK and mitochondrial processing peptidase. *Circ Res* 115: 450–459, 2014. doi:10.1161/CIRCRESAHA.115.304262.

33. **Peyton KJ, Ensenat D, Azam MA, Keswani AN, Kannan S, Liu XM, Wang H, Tulis DA, Durante W.** Arginase promotes neointima formation in rat injured carotid arteries. *Arterioscler Thromb Vasc Biol* 29: 488–494, 2009. doi:10.1161/ATVBAHA.108.183392.

34. **Qin Z, Hou X, Weisbrod RM, Seta F, Cohen RA, Tong X.** Nox2 mediates high fat high sucrose diet-induced nitric oxide dysfunction and inflammation in aortic smooth muscle cells. *J Mol Cell Cardiol* 72: 56–63, 2014. doi:10.1016/j.yjmcc.2014.02.019.

35. **Qiu S, Mintz JD, Salet CD, Han W, Giannis A, Chen F, Yu Y, Su Y, Fulton DJ, Stepp DW.** Increasing muscle mass improves vascular function in obese (db/db) mice. *J Am Heart Assoc* 3: e000854, 2014. doi:10.1161/JAHA.114.000854.

36. **Ran FA, Hsu PD, Wright J, Agarwala V, Scott DA, Zhang F.** Genome engineering using the CRISPR-Cas9 system. *Nat Protoc* 8: 2281–2308, 2013. doi:10.1038/nprot.2013.143.

37. **Romero MJ, Platt DH, Tawfik HE, Labazi M, El-Remessy AB, Bartoli M, Caldwell RB, Caldwell RW.** Diabetes-induced coronary vascular dysfunction involves increased arginase activity. *Circ Res* 102: 95–102, 2008. doi:10.1161/CIRCRESAHA.107.155028.

38. **Safar ME, Balkau B, Lange C, Protogerou AD, Czernichow S, Blacher J, Levy BI, Smulyan H.** Hypertension and vascular dynamics in men and women with metabolic syndrome. *J Am Coll Cardiol* 61: 12–19, 2013. doi:10.1016/j.jacc.2012.01.088.

39. **Shi C, Pamer EG.** Monocyte recruitment during infection and inflammation. *Nat Rev Immunol* 11: 762–774, 2011. doi:10.1038/nri3070.

40. **Southan GJ, Szabó C.** Selective pharmacological inhibition of distinct nitric oxide synthase isoforms. *Biochem Pharmacol* 51: 383–394, 1996. doi:10.1016/0006-2952(95)02099-3.

41. **Tarín C, Gomez M, Calvo E, López JA, Zaragoza C.** Endothelial nitric oxide deficiency reduces MMP-13-mediated cleavage of ICAM-1 in vascular endothelium: a role in atherosclerosis. *Arterioscler Thromb Vasc Biol* 29: 27–32, 2009. doi:10.1161/ATVBAHA.108.169623.

42. **Taşcă C, Stefăneanu L, Vasilescu C.** The myocardial microangiopathy in human and experimental diabetes mellitus. (A microscopic, ultrastructural, morphometric and computer-assisted symbolic-logic analysis). *Endocrinologie* 24: 59–69, 1986.

43. **van Greevenbroek MM, Schalkwijk CG, Stehouwer CD.** Obesity-associated low-grade inflammation in type 2 diabetes mellitus: causes and consequences. *Neth J Med* 71: 174–187, 2013.

44. **Wang L, Bhatta A, Toque HA, Rojas M, Yao L, Xu Z, Patel C, Caldwell RB, Caldwell RW.** Arginase inhibition enhances angiogenesis in endothelial cells exposed to hypoxia. *Microvasc Res* 98: 1–8, 2015. doi:10.1016/j.mvr.2014.11.002.

45. **Weisberg SP, McCann D, Desai M, Rosenbaum M, Leibel RL, Ferrante AW Jr.** Obesity is associated with macrophage accumulation in adipose tissue. *J Clin Invest* 112: 1796–1808, 2003. doi:10.1172/JCI200319246.

46. **Weisbrod RM, Shiang T, Al Sayah L, Fry JL, Bajpai S, Reinhart-King CA, Lob HE, Santhanam L, Mitchell G, Cohen RA, Seta F.** Arterial stiffening precedes systolic hypertension in diet-induced obesity. *Hypertension* 62: 1105–1110, 2013. doi:10.1161/HYPERTENSIONAHA.113.01744.

47. **World Health Organization.** *Obesity and Overweight Fact Sheet* (Online). http://www.who.int/mediacentre/factsheets/fs311/en/. [29 May 2016].

48. **Xu H, Barnes GT, Yang Q, Tan G, Yang D, Chou CJ, Sole J, Nichols A, Ross JS, Tartaglia LA, Chen H.** Chronic inflammation in fat plays a crucial role in the development of obesity-related insulin resistance. *J Clin Invest* 112: 1821–1830, 2003. doi:10.1172/JCI200319451.

49. **Yang J, Zhang L, Yu C, Yang XF, Wang H.** Monocyte and macrophage differentiation: circulation inflammatory monocyte as biomarker for inflammatory diseases. *Biomark Res* 2: 1, 2014. doi:10.1186/2050-7771-2-1.

50. **Yang Z, Ming XF.** Functions of arginase isoforms in macrophage inflammatory responses: impact on cardiovascular diseases and metabolic disorders. *Front Immunol* 5: 533, 2014. doi:10.3389/fimmu.2014.00533.

51. **Zeiher AM, Fisslthaler B, Schray-Utz B, Busse R.** Nitric oxide modulates the expression of monocyte chemoattractant protein 1 in cultured human endothelial cells. *Circ Res* 76: 980–986, 1995. doi:10.1161/01.RES.76.6.980.

52. **Zhang C, Wu J, Xu X, Potter BJ, Gao X.** Direct relationship between levels of TNF-alpha expression and endothelial dysfunction in reperfusion injury. *Basic Res Cardiol* 105: 453–464, 2010. doi:10.1007/s00395-010-0083-6.

53. **Zhang D, Fang P, Jiang X, Nelson J, Moore JK, Kruger WD, Berretta RM, Houser SR, Yang X, Wang H.** Severe hyperhomocysteinemia promotes bone marrow-derived and resident inflammatory monocyte differentiation and atherosclerosis in LDLr/CBS-deficient mice. *Circ Res* 111: 37–49, 2012. doi:10.1161/CIRCRESAHA.112.269472.